AIMS Mathematics, 6 (7): 7056–7069.
DOI: 10.3934/math.2021414
Received: 23 March 2021
Accepted: 21 April 2021
Published: 27 April 2021

http://www.aimspress.com/journal/Math

Research article

On the supporting nodes in the localized method of fundamental solutions for 2D potential problems with Dirichlet boundary condition

Zengtao Chen[1] and Fajie Wang[1,2,*]

[1] College of Mechanical and Electrical Engineering, National Engineering Research Center for Intelligent Electrical Vehicle Power System, Qingdao University, Qingdao 266071, China
[2] Institute of Mechanics for Multifunctional Materials and Structures, Qingdao University, Qingdao 266071, China

* **Correspondence:** Email: wfj1218@126.com; Tel: +86053285953800; Fax: +86053285953800.

Abstract: This paper proposes a simple, accurate and effective empirical formula to determine the number of supporting nodes in a newly-developed method, the localized method of fundamental solutions (LMFS). The LMFS has the merits of meshless, high-accuracy and easy-to-simulation in large-scale problems, but the number of supporting nodes has a certain impact on the accuracy and stability of the scheme. By using the curve fitting technique, this study established a simple formula between the number of supporting nodes and the node spacing. Based on the developed formula, the reasonable number of supporting nodes can be determined according to the node spacing. Numerical experiments confirmed the validity of the proposed methodology. This paper perfected the theory of the LMFS, and provided a quantitative selection strategy of method parameters.

Keywords: localized method of fundamental solutions; supporting nodes; empirical formula; potential problems; meshless method
Mathematics Subject Classification: 35J05, 65N35, 68W99

1. Introduction

The method of fundamental solutions (MFS) [1,2] is a simple, accurate and efficient boundary-type meshfree approach for the solution of partial differential equations, which uses the fundamental solution of a differential operator as a basis function. Chen et al. [3,4] demonstrated the equivalence between the MFS and the Trefftz collocation method [5] under certain conditions.

During the last decades, the MFS has been widely applied to various fields in applied mathematics and mechanics, such as scattering and radiation problems [6], inverse problems [7], non-linear problems [8], and fractal derivative models [9,10]. For more details and applications, the readers are referred to Refs. [11–13] and the references therein. In the MFS, the approximation solution is assumed as a linear combination of fundamental solutions. In order to avoid the source singularity of the fundamental solution, this method requires a fictitious boundary outside the computational domain, and places the source points on it. The distance between the fictitious boundary and the real boundary has a certain influence on the calculation accuracy [14–16]. To address this issue, many scholars proposed improved methods, such as the singular boundary method [17,18], modified method of fundamental solutions [19], the non-singular method of fundamental solutions [20]. Due to the characteristic of dense matrix, the traditional and improved MFS with "global" discretization is difficult to apply in the large-scale problems with complicated geometries.

Recently, Fan and Chen et al. [21] proposed an improved version of traditional MFS, known as the localized method of fundamental solutions (LMFS), for solving Laplace and biharmonic equations. The LMFS is essentially a localized semi-analytical meshless collocation scheme, and overcomes the limitation of traditional method in applications of complex geometry and large-scale problems. Gu and Liu et al. [22–25] extended to the LMFS to elasticity, heat conduction and inhomogeneous elliptic problems. Qu et al. [26–28] applied the method to the interior acoustic and bending analysis. Wang et al. [29–32] developed the localized space-time method of fundamental solutions, and resolved the inverse problems. Li et al. [33] used this method to simulate 2D harmonic elastic wave problems. Liu et al. [34] combined the LMFS and the Crank-Nicolson time-stepping technology to address the transient convection-diffusion-reaction equations. Li, Qu and Wang et al. [35–37] given the error analysis of the LMFS, and proposed a augmented moving least squares approximation. Like the element-free Galerkin method [38,39] being successfully applied to a large number of partial differential equations, the proposed LMFS belongs to the domain-type meshless method. Unlike the former, the latter is a semi-analytical meshless collocation method with strong form, in which the fundamental solutions are unavoidable. In the LMFS, the whole computational domain is firstly divided into a set of overlapping local subdomains whose boundary could be a circle (for 2D problems) and/or a sphere (for 3D problems). In each of the local subdomain, the classical MFS formulation and the moving least square (MLS) method are applied to the local approximation of variables. This method remains the high accuracy of the traditional MFS, and simultaneously produces a sparse system of linear algebraic equations. Inspired by the LMFS, recently, some new local meshless methods [40–44] have also been proposed.

No methodology is perfect, although the LMFS has achieved varying degrees of success in various fields, it still faces some thorny problems to be solved. As a local semi-analytical meshless technique, the LMFS needs to configure nodes in the whole computational domain and to select the supporting nodes in each local subdomain, which likes the generalized finite difference method [45–47]. The node spacing (related to the total number of nodes), the number of supporting nodes and the relationship between them have the certain influence on the accuracy. Fu et al. [48] discussed the selection algorithm of supporting nodes in the generalized finite difference method. However, there are few reports in the literature coordinating the node spacing and the number of supporting nodes in the LMFS.

In this paper, we propose an effective empirical formula to determine the node spacing and the number of supporting nodes in the LMFS for solving 2D potential problems with Dirichlet boundary

condition. A reasonable number of supporting nodes can be directly given according to the size of node spacing. The proposed methodology is applicable to both regular and irregular distribution of nodes in arbitrary domain. This study consummates the LMFS and lays a foundation for simulating various engineering problems accurately and stably.

The rest of paper is organized as follows. In Section 2, we give the governing equation and boundary condition of 2D potential problems, and provide the numerical implementation of LMFS. Section 3 introduces the empirical formula of the node spacing and the number of supporting nodes in the LMFS. Section 4 investigates two numerical examples with irregular domain and nodes to illustrate the accuracy and reliability of the empirical formula. Section 5 summarizes some conclusions.

2. The LMFS for 2D potential problems

Considering the following 2D potential problem with the Dirichlet boundary condition:

$$\nabla^2 u(x,y)=0, \quad (x,y)\in\Omega, \tag{1}$$

$$u=\bar{u}(x,y), \quad (x,y)\in\Gamma, \tag{2}$$

where ∇^2 is the 2D Laplacian, $u(x,y)$ the unknown variable, Ω the computational domain, $\Gamma=\partial\Omega$ the boundary of domain, and $\bar{u}(x,y)$ the given function.

According to the ideas of the LMFS, $N=ni+nb$ nodes $\boldsymbol{x}^i$ $(i=1,2,...,N)$ should be distributed inside the considered domain Ω and along its boundary Γ, where *ni* is the number of interior nodes, *nb* is the number of boundary nodes. Consider an arbitrary node $\boldsymbol{x}^{(0)}$ (called the central node), we can find *m* supporting nodes $\boldsymbol{x}^{(i)}$ $(i=1,2,...,m)$ around the central node $\boldsymbol{x}^{(0)}$ (see Figure 1 (a)). At the same time, the local subdomain Ω_s can also be defined. Subsequently, the MFS formulation is implemented for the local subdomain. For this purpose, an artificial boundary $\widehat{\Omega}_s$ is selected at a certain distance from the boundary of local subdomain, as shown in Figure 1 (b). On the artificial boundary, M uniformly distributed source points are specified.

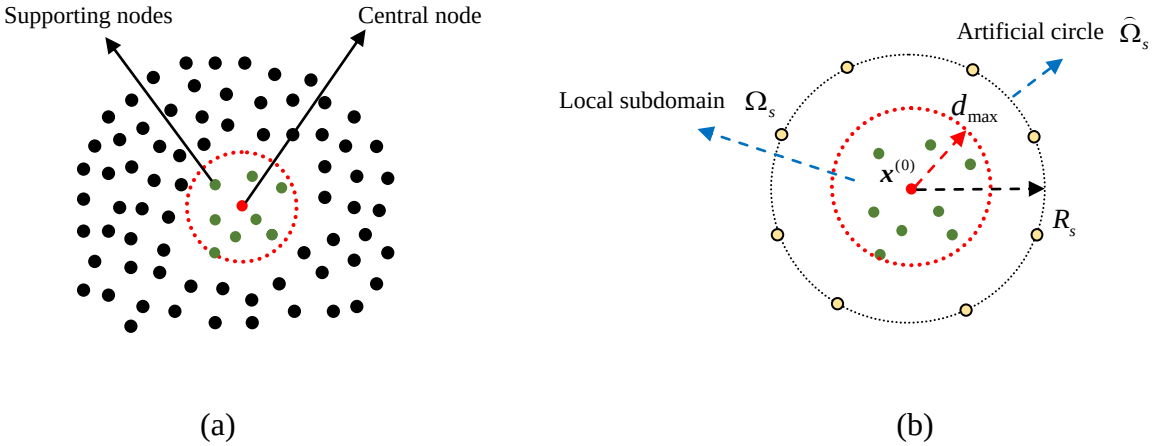

Figure 1. Schematic diagram of the LMFS: (a) nodal distribution and (b) local subdomain.

For each node in the local subdomain Ω_s, the following MFS formulation of numerical solution should be hold

$$u(\boldsymbol{x}^{(i)}) = \sum_{j=1}^{M} \alpha_j G(\boldsymbol{x}^{(i)}, \boldsymbol{s}^{(j)}),\ \boldsymbol{x}^{(i)} \in \Omega_s,\ i = 0,1,...,m, \tag{3}$$

or for brevity

$$u^{(i)} = \sum_{j=1}^{M} \alpha_j G_{ij} = \boldsymbol{G}^{(i)}\boldsymbol{\alpha},\ \boldsymbol{x}^{(i)} \in \Omega_s,\ i = 0,1,...,m, \tag{4}$$

where $(\boldsymbol{x}^{(i)})_{i=0}^{m}$ are the $m+1$ nodes in the subdomains Ω_s, $(\boldsymbol{s}^{(j)})_{j=1}^{M}$ denote M fictitious source points, $\boldsymbol{\alpha} = (\alpha_1, \alpha_2, \ldots, \alpha_M)^T$ represent the unknown coefficient vector, $G_{ij} = G(\boldsymbol{x}^{(i)}, \boldsymbol{s}^{(j)})$ are the fundamental solutions expressed as

$$G(\boldsymbol{x}^{(i)}, \boldsymbol{s}^{(j)}) = -\frac{1}{2\pi} \ln \left\| \boldsymbol{x}^{(i)}, \boldsymbol{s}^{(j)} \right\|_2 . \tag{5}$$

It should be pointed out that the artificial boundary is a circle centered at $\boldsymbol{x}^{(0)}$ and with radius R_s (see Figure 1 (b)), here R_s is a parameter that should be manually fixed by the user.

In each local subdomain, we determine the unknown coefficients $(\alpha_j)_{j=1}^{M}$ in Eq (3) or (4) by the moving least square (MLS) method, we can define a residual function as follows

$$B(\boldsymbol{\alpha}) = \sum_{i=0}^{m} \left[\boldsymbol{G}^{(i)}\boldsymbol{\alpha} - u^{(i)} \right]^2 \omega^{(i)}, \tag{6}$$

in which $\omega^{(i)}$ represents the weighting function related with node $\boldsymbol{x}^{(i)}$ and is introduced as [49]

$$\omega^{(i)} = \frac{\exp\left[-(d_i / h)^2\right] - \exp\left[-(d_{\max} / h)^2\right]}{1 - \exp\left[-(d_{\max} / h)^2\right]},\ i = 0,1,\ldots,m, \tag{7}$$

where $d_i = \left\| \boldsymbol{x}^{(i)} - \boldsymbol{x}^{(0)} \right\|_2$ denotes the distance of the central node and its *i*th supporting node, $d_{\max}$ is the size of the local subdomain (the maximum value of distances between $\boldsymbol{x}^{(0)}$ and *m* supporting nodes, i.e., $d_{\max} = \max_{i=1,2,\ldots,m} \left(d_i\right)$), and $h = 1$.

Based on the MLS approximation, we can get the coefficient vector $\boldsymbol{\alpha} = (\alpha_1, \alpha_2, \cdots, \alpha_M)^T$ by minimizing $B(\boldsymbol{\alpha})$ with respect to $\boldsymbol{\alpha}$ as follows

$$\frac{\partial B(\boldsymbol{\alpha})}{\partial \alpha_j} = 0,\ j=1,2,\ldots,M, \tag{8}$$

Then, a linear system can be formed

$$\boldsymbol{A}\boldsymbol{\alpha}=\boldsymbol{b}, \tag{9}$$

where

$$\boldsymbol{A}=\begin{bmatrix} \sum_{i=0}^{m}G_{i1}^2\omega^{(i)} & \sum_{i=0}^{m}G_{i1}G_{i2}\omega^{(i)} & \sum_{i=0}^{m}G_{i1}G_{i3}\omega^{(i)} & \cdots & \sum_{i=0}^{m}G_{i1}G_{iM}\omega^{(i)} \\ & \sum_{i=0}^{m}G_{i2}^2\omega^{(i)} & \sum_{i=0}^{m}G_{i2}G_{i3}\omega^{(i)} & \cdots & \sum_{i=0}^{m}G_{i2}G_{iM}\omega^{(i)} \\ & & \sum_{i=0}^{m}G_{i3}^2\omega^{(i)} & \cdots & \sum_{i=0}^{m}G_{i3}G_{iM}\omega^{(i)} \\ & SYM & & \ddots & \vdots \\ & & & & \sum_{i=0}^{m}G_{iM}^2\omega^{(i)} \end{bmatrix},\ \boldsymbol{b}=\begin{bmatrix} \sum_{i=0}^{m}G_{i1}\omega^{(i)}u^{(i)} \\ \sum_{i=0}^{m}G_{i2}\omega^{(i)}u^{(i)} \\ \sum_{i=0}^{m}G_{i3}\omega^{(i)}u^{(i)} \\ \vdots \\ \sum_{i=0}^{m}G_{iM}\omega^{(i)}u^{(i)} \end{bmatrix}. \tag{10}$$

The vector $\boldsymbol{b}$ in Eq (10) can be further expressed as

$$\boldsymbol{b}=\begin{bmatrix} G_{01}\omega^{(0)} & G_{11}\omega^{(1)} & \cdots & G_{m1}\omega^{(m)} \\ G_{02}\omega^{(0)} & G_{12}\omega^{(1)} & \cdots & G_{m2}\omega^{(m)} \\ \vdots & \vdots & \ddots & \vdots \\ G_{0M}\omega^{(0)} & G_{1M}\omega^{(1)} & \cdots & G_{mM}\omega^{(m)} \end{bmatrix}\begin{pmatrix} u^{(0)} \\ u^{(1)} \\ \vdots \\ u^{(m)} \end{pmatrix}=\boldsymbol{B}\begin{pmatrix} u^{(0)} \\ u^{(1)} \\ \vdots \\ u^{(m)} \end{pmatrix}. \tag{11}$$

According to Eqs (9)–(11), the unknown coefficients $\boldsymbol{\alpha}=(\alpha_1,\alpha_2,\ldots,\alpha_M)^T$ can now be calculated as

$$\boldsymbol{\alpha}=\begin{pmatrix} \alpha_1 \\ \alpha_2 \\ \vdots \\ \alpha_M \end{pmatrix}=\boldsymbol{A}^{-1}\boldsymbol{B}\begin{pmatrix} u^{(0)} \\ u^{(1)} \\ \vdots \\ u^{(m)} \end{pmatrix}. \tag{12}$$

To ensure the regularity of matrix $\boldsymbol{A}$ in Eq (12), $m+1$ should be greater than M. For simplicity, we fixed $m+1=2M$ in the computations. It should be pointed out that the matrix $\boldsymbol{A}$ with a small size given in Eq (10) is well-conditioned. In this study, the MATLAB routine "$\boldsymbol{A}\backslash\boldsymbol{B}$" is used to calculate $\boldsymbol{A}^{-1}\boldsymbol{B}$ in order to avoid the troublesome matrix inversion.

Substituting Eq (12) into Eq (4) as $i=0$, the numerical solution at central node $\boldsymbol{x}^{(0)}$ is expressed as

$$u^{(0)}=\boldsymbol{G}^{(0)}\boldsymbol{\alpha}=\boldsymbol{G}^{(0)}\boldsymbol{A}^{-1}\boldsymbol{B}\begin{pmatrix} u^{(0)} \\ u^{(1)} \\ \vdots \\ u^{(m)} \end{pmatrix}=\sum_{j=0}^{m}c^{(j)}u^{(j)}, \tag{13}$$

or

$$u^{(0)} - \sum_{j=0}^{m} c^{(j)} u^{(j)} = 0, \tag{14}$$

in which $(c^{(j)})_{j=0}^{m}$ are coefficients which can be calculated by $\boldsymbol{G}^{(0)}\boldsymbol{A}^{-1}\boldsymbol{B}$.

Now we can obtained a final linear algebraic equation system of the LMFS according to the governing equation and boundary condition. At interior nodes, the physical quantities must satisfy the governing equation, namely,

$$u^{i} - \sum_{j=0}^{m} c_i^{(j)} u^{(j)} = 0, \quad i=1,2,\ldots,ni, \tag{15}$$

where subscript i of $c_i^{(j)}$ is used to distinguish the coefficients for different interior nodes. At boundary nodes with Dirichlet boundary condition, we have

$$u^{i} = \bar{u}^{i}, \quad i = ni+1, ni+2, \ldots, ni+nd. \tag{16}$$

Using the given boundary data and combing Eqs (15) and (16), we have the following sparse system of linear algebraic equations

$$\boldsymbol{C}\boldsymbol{U} = \boldsymbol{f}, \tag{17}$$

where $\boldsymbol{C}_{N\times N}$ represents the coefficient matrix, $\boldsymbol{U} = (u^1, u^2, \ldots, u^N)^T$ denotes the undetermined vector of variables at all nodes, and $\boldsymbol{f}_{N\times 1}$ is a known vector composed by given boundary condition and zero vector. It should be pointed out that the system given in Eq (17) is well-conditioned, and standard solvers can be used to obtain its solution. In this study, the MATLAB routine "$\boldsymbol{U} = \boldsymbol{C} \setminus \boldsymbol{f}$" is used to solve this system of equation. After solving Eq (17), the approximated solutions at all nodes can be acquired.

3. Experiential formula of the supporting nodes in the LMFS

In this section, three different analytical solutions are provided to summarize the relationship between the number of supporting nodes (m) and the node spacing (Δh). Without loss of generality, the node spacing is defined by

$$\Delta h = \max_{1\le i\le N} \min_{1\le j\le N} \left| \boldsymbol{x}^i - \boldsymbol{x}^j \right|. \tag{18}$$

Noted that the node spacing is equivalent to the total number of nodes, and is suitable for the arbitrary distribution of nodes including regular and irregular distributions. In the investigation, the equidistant nodes are used, thus the node spacing Δh is the distance between two adjacent nodes. In all calculations, the artificial radius is fixed with $R_s = 1.5$, and the numerical results are calculated on a computer equipped with i5-5200 CPU@2.20GHz and 4GB memory. To estimate the accuracy of

the present scheme, we adopt the root-mean-square error (*RMSE*) defined by

$$RMSE = \sqrt{\frac{1}{N_{total}} \sum_{k}^{N_{total}} \left(u_{num}(\boldsymbol{x}^k) - u_{exa}(\boldsymbol{x}^k) \right)^2}, \tag{19}$$

where $u_{num}(\boldsymbol{x}^k)$ and $u_{exa}(\boldsymbol{x}^k)$ are the numerical and analytical solutions at kth test points respectively, N_{total} is the total number of tested points, which refers to all nodes unless otherwise specified.

As shown in Figure 2, a rectangular with equidistant nodes is considered. To obtain a relatively universal formula, three different exact solutions are employed, as shown below:

$$u(x, y) = x^2 - y^2, \tag{20}$$

$$u(x, y) = \sin(x)\mathrm{e}^y, \tag{21}$$

$$u(x, y) = \cos(x)\cosh(y) + \sin(x)\sinh(y). \tag{22}$$

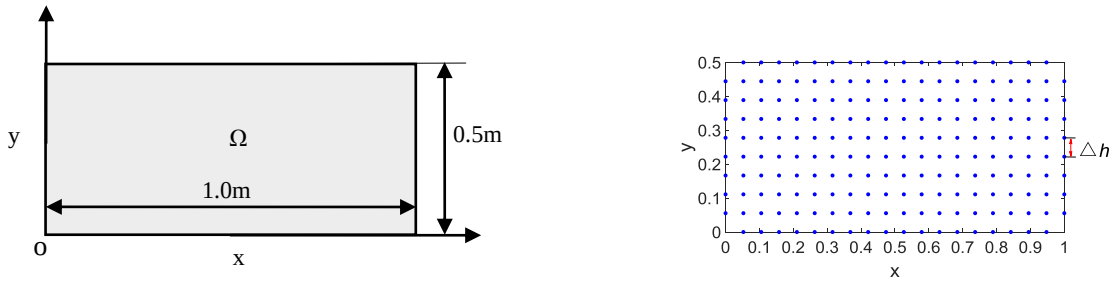

(a) Computational domain (b) Nodal distribution

Figure 2. Computational domain and nodal distribution.

In order to numerically analyze the relationship between m and Δh, we choose different m and Δh, and draw the *RMSE* profiles obtained by the LMFS. For the analytical solution in Eq (20), the fitting curve can be formulated as $m = \lceil a \cdot \Delta h^{(b)} \rceil$ ($\lceil \cdot \rceil$ denotes the round up operation), where $2.057 < a < 3.759$ and $-0.305 < b < -0.1509$. Figure 3 plots the case with $a = 3$ and $b = -0.22$. For the analytical solution in Eq (21), the fitting curve can be formulated as $m = \lceil a \cdot \Delta h^{(b)} \rceil$, where $2.221 < a < 3.314$ and $-0.2817 < b < -0.1765$. Figure 4 plots the case with $a = 2.76$ and $b = -0.23$. For the analytical solution in Eq (22), the fitting curve can be formulated as $m = \lceil a \cdot \Delta h^{(b)} \rceil$, where $2.61 < a < 3.153$ and $-0.2437 < b < -0.1937$. Figure 5 plots the case with $a = 2.85$ and $b = -0.22$.

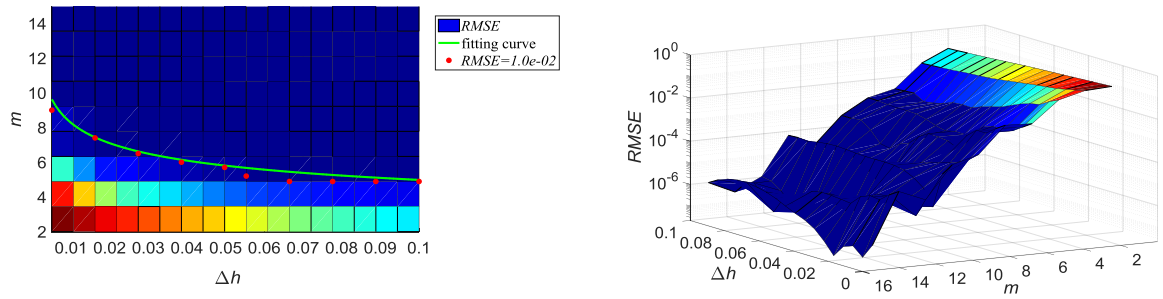

(a) 2D error plane (b) 3D error surface

Figure 3. Distribution of *RMSE*s under different m and Δh.

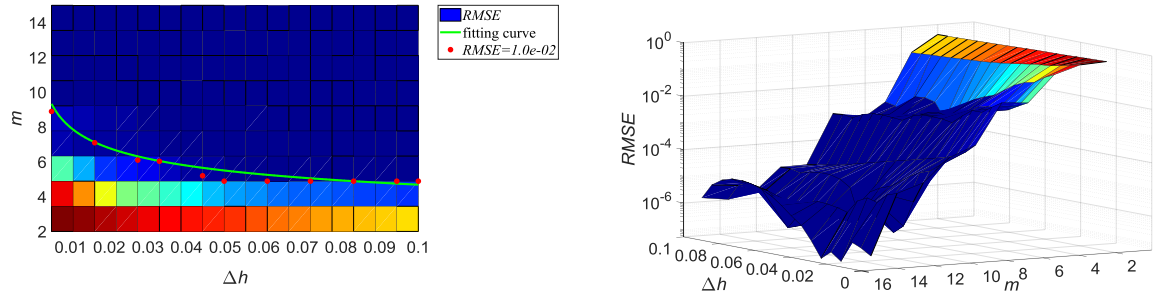

(a) 2D error plane (b) 3D error surface

Figure 4. Distribution of *RMSE*s under different m and Δh.

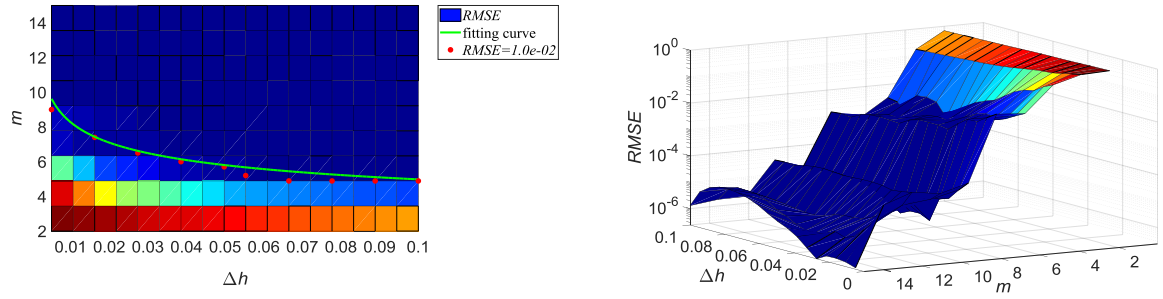

(a) 2D error plane (b) 3D error surface

Figure 5. Distribution of *RMSE*s under different m and Δh.

By considering the above three cases for different analytical solutions, the following simple empirical formula can be carefully concluded:

$$m = \left\lceil 3 \cdot \Delta h^{(-0.22)} \right\rceil. \tag{23}$$

From Eq (23), we can easily determine the number of supporting nodes by the node spacing. In the next section, two complex examples will be provided to verify the present expression.

4. Numerical experiments

This section tests two numerical examples with complex boundaries. The following three different analytical solutions are used to to carefully validate the reliability of the empirical formula.

$$u = \sin(x)\mathrm{e}^{y}, \tag{24}$$

$$u = \cos(x)\cosh(y) + \sin(x)\sinh(y), \tag{25}$$

$$u = \cos(x)\cosh(y) + x^2 - y^2 + 2x + 3y + 1. \tag{26}$$

***Example 1*:**

A gear-shaped domain is considered as shown in Figure 6. The LMFS uses 1334 nodes including 1134 internal nodes and 200 boundary nodes generated from the MATLAB codes, The node spacing is $\Delta h = 0.0667\mathrm{m}$ calculated from Eq (18). It can be known from the empirical formula (23) that the number of supporting nodes should be $m \geq 6$, when the numerical error remains $RMSE \leq 1.0\mathrm{e}-02$.

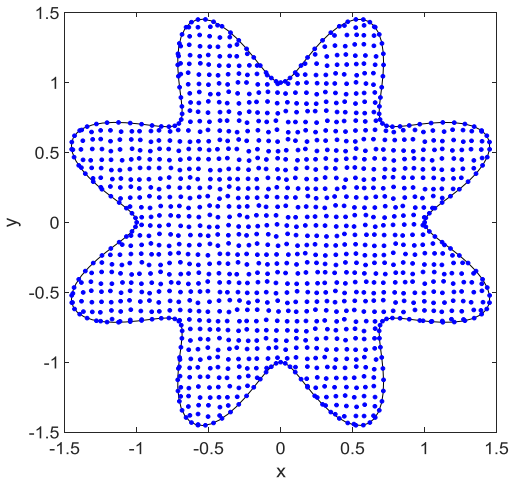

Figure 6. Distribution of nodes on the gear-shaped model.

Figure 7 illustrates the *RMSE*s of numerical solutions at all nodes with respect to the number of supporting nodes for the different analytical solutions, where A, B and C represent the analytical solutions (24), (25) and (26), respectively. As can be seen, the numerical results for different types of exact solutions converge with increasing number of supporting nodes. More importantly, it can be observed from Figure 7 that $RMSE \leq 1.0\mathrm{e}-02$ when $m \geq 6$, indicating the reliability and accuracy of the proposed empirical formula.

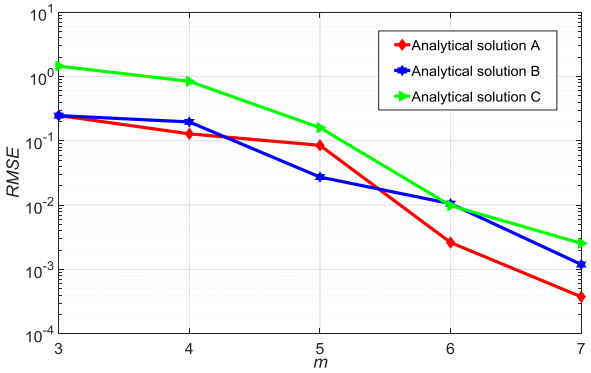

Figure 7. Error curves of the LMFS under different number of supporting nodes.

Example 2:

In the second example, we consider a car cavity model. Figure 8 shows the problem geometry and the distribution of nodes. The total number of nodes is $N = 11558$, including 11212 internal nodes and 346 boundary nodes. Nodes in this model are derived from the *HyperMesh* software. The node spacing is $\Delta h = 0.02\text{m}$ calculated from Eq (18). It should be pointed out that According to the proposed empirical formula (23), the number of supporting nodes needs to meet $m \geq 8$ when the numerical error remains $RMSE \leq 1.0\text{e}-02$.

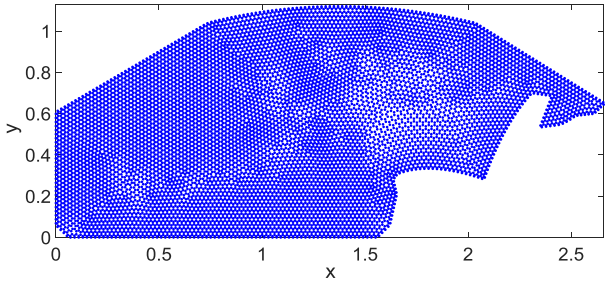

Figure 8. Geometry of the problem and the distribution of nodes.

Figure 9 depicts error curves of the LMFS with the increase of the number of supporting nodes, under deferent tested solutions. Despite the complicated domain and the irregular-distributed nodes, the results in Figure 9 are in good agreement with our empirical formula. The above numerical results fully demonstrate the reliability of the present methodology. It is worth mentioning that a large number of numerical experiments have been performed with the empirical formula in Eq (23), and all experiments observe the similar performance.

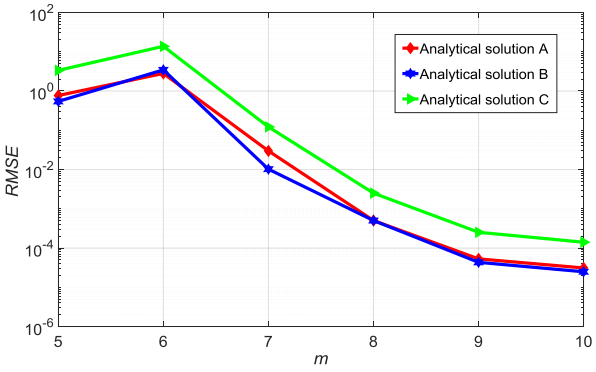

Figure 9. Error curves of the LMFS under different number of supporting nodes.

5. Conclusions

In this paper, a simple, accurate and effective empirical formula is proposed to choose the number of supporting nodes. As a local collocation method, the number of supporting nodes has an important impact on the accuracy of the LMFS. This study given the direct relationship between the number of supporting nodes and the node spacing. By using the proposed formula, a reasonable number of supporting nodes can be determined according to the node spacing. Numerical results demonstrate the validity of the developed formula. The proposed empirical formula is beneficial to accuracy, simplicity and university for selecting the number of supporting nodes in the LMFS. This paper perfected the theory of the LMFS, and provided a quantitative selection strategy of method parameters.

It should be noted that the present study focuses on the 2D homogeneous linear potential problems with Dirichlet boundary condition. The proposed formula can not be directly applied to the 2D cases with Neumann boundary and 3D cases with Dirichlet or Neumann boundary condition. In addition, the LMFS depends on the fundamental solutions of governing equations. For the nonhomogeneous and/or nonlinear problems without the fundamental solutions, the appropriate auxiliary technologies should be introduced in the LMFS, and then the corresponding formula still need for further study. The subsequent works will be emphasized on these issues, according to the idea developed in this paper.

Acknowledgments

The work described in this paper was supported by the Natural Science Foundation of Shandong Province of China (No. ZR2019BA008), the China Postdoctoral Science Foundation (No. 2019M652315), the National Natural Science Foundation of China (Nos.11802151, 11802165, 11872220), and Qingdao People's Livelihood Science and Technology Project (No. 19-6-1-88-nsh).

Conflict of interest

The authors declare that they have no conflicts of interest to report regarding the present study.

References

1. G. Fairweather, A. Karageorghis, The method of fundamental solutions for elliptic boundary value problems, *Adv. Comput. Math.*, **9** (1998), 69–95.
2. M. A. Golberg, C. S. Chen, The method of fundamental solutions for potential, Helmholtz and diffusion problems, In: *Boundary Integral Methods-Numerical and Mathematical Aspects* (Ed. M. A. Golberg), (1999), 103–176.
3. J. T. Chen, C. S. Wu, Y. T. Lee, K. H. Chen, On the equivalence of the Trefftz method and method of fundamental solutions for Laplace and biharmonic equations, *Comput. Math. Appl.*, **53** (2007), 851–879.
4. J. T. Chen, Y. T. Lee, S. R. Yu, S. C. Shieh, Equivalence between the Trefftz method and the method of fundamental solution for the annular Green's function using the addition theorem and image concept, *Eng. Anal. Bound. Elem.*, **33** (2009), 678–688.
5. J. A. Kołodziej, J. K. Grabski, Many names of the Trefftz method, *Eng. Anal. Bound. Elem.*, **96** (2018), 169–178.
6. G. Fairweather, A. Karageorghis, P. A. Martin, The method of fundamental solutions for scattering and radiation problems, *Eng. Anal. Bound. Elem.*, **27** (2003), 759–769.
7. Y. C. Hon, T. Wei, A fundamental solution method for inverse heat conduction problem, *Eng. Anal. Bound. Elem.*, **28** (2004), 489–495.
8. C. S. Chen, The method of fundamental solutions for non-linear thermal explosions, *Commun. Numer. Methods Eng.*, **11** (1995), 675–681.
9. F. J. Wang, W. Cai, B. Zheng, C. Wang, Derivation and numerical validation of the fundamental solutions for constant and variable-order structural derivative advection-dispersion models, *Z. Angew. Math. Phys.*, **71** (2020), 135.
10. W. Cai, F. J. Wang, Numerical investigation of three-dimensional hausdorff derivative anomalous diffusion model, *Fractals*, **28** (2020), 2050020.
11. A. H. D. Cheng, Y. Hong, An overview of the method of fundamental solutions-Solvability, uniqueness, convergence, and stability, *Eng. Anal. Bound. Elem.*, **120** (2020), 118–152.
12. F. F. Dou, L. P. Zhang, Z. C. Li, C. S. Chen, Source nodes on elliptic pseudo-boundaries in the method of fundamental solutions for Laplace's equation; selection of pseudo-boundaries, *J. Comput. Appl. Math.*, **377** (2020), 112861.
13. M. R. Hematiyan, M. Mohammadi, C. C. Tsai, The method of fundamental solutions for anisotropic thermoelastic problems, *Appl. Math. Model.*, **95** (2021), 200–218.
14. C. J. S. Alves, On the choice of source points in the method of fundamental solutions, *Eng. Anal. Bound. Elem.*, **33** (2009), 1348–1361.
15. F. J. Wang, C. S. Liu, W. Z. Qu, Optimal sources in the MFS by minimizing a new merit function: Energy gap functional, *Appl. Math. Lett.*, **86** (2018), 229–235.
16. J. K. Grabski, On the sources placement in the method of fundamental solutions for time-dependent heat conduction problems, *Comput. Math. Appl.*, **88** (2021), 33–51.
17. W. Chen, F. J. Wang, A method of fundamental solutions without fictitious boundary, *Eng. Anal. Bound. Elem.*, **34** (2010), 530–532.
18. L. Qiu, F. J. Wang, J. Lin, Y. Zhang, A meshless singular boundary method for transient heat conduction problems in layered materials, *Comput. Math. Appl.*, **78** (2019), 3544–3562.

19. D. L. Young, K. H. Chen, J. T. Chen, J. H. Kao, A modified method of fundamental solutions with source on the boundary for solving Laplace equations with circular and arbitrary domains, Cmes-*Comp. Model. Eng. Sci.*, **19** (2007), 197–221.
20. Q. G. Liu, B. Šarler, Non-singular method of fundamental solutions for anisotropic elasticity, *Eng. Anal. Bound. Elem.*, **45** (2014), 68–78.
21. C. M. Fan, Y. K. Huang, C. S. Chen, S. R. Kuo, Localized method of fundamental solutions for solving two-dimensional Laplace and biharmonic equations, *Eng. Anal. Bound. Elem.*, **101** (2019), 188–197.
22. Y. Gu, C. M. Fan, R. P. Xu, Localized method of fundamental solutions for large-scale modelling of two-dimensional elasticity problems, *Appl. Math. Lett.*, **93** (2019), 8–14.
23. Y. Gu, C. M. Fan, W. Z. Qu, F. J. Wang, Localized method of fundamental solutions for large-scale modelling of three-dimensional anisotropic heat conduction problems-Theory and MATLAB code, *Comput. Struct.*, **220** (2019), 144–155.
24. Y. Gu, C. M. Fan, W. Z. Qu, Localized method of fundamental solutions for three-dimensional inhomogeneous elliptic problems: Theory and MATLAB code, *Comput. Mech.*, **64** (2019), 1567–1588.
25. Q. G. Liu, C. M. Fan, B. Šarler, Localized method of fundamental solutions for two-dimensional anisotropic elasticity problems, *Eng. Anal. Bound. Elem.*, **125** (2021), 59–65.
26. W. Z. Qu, C. M. Fan, Y. Gu, F. J. Wang, Analysis of three-dimensional interior acoustic fields by using the localized method of fundamental solutions, *Appl. Math. Model.*, **76** (2019), 122–132.
27. W. Z. Qu, L. L. Sun, P. W. Li, Bending analysis of simply supported and clamped thin elastic plates by using a modified version of the LMFS, *Math. Comput. Simulat.*, **185** (2021), 347–357.
28. W. Z. Qu, C. M. Fan, Y. Gu, Localized method of fundamental solutions for interior Helmholtz problems with high wave number, *Eng. Anal. Bound. Elem.*, **107** (2019), 25–32.
29. F. J. Wang, C. M. Fan, Q. S. Hua, Y. Gu, Localized MFS for the inverse Cauchy problems of two-dimensional Laplace and biharmonic equations, *Appl. Math. Comput.*, **364** (2020), 124658.
30. F. J. Wang, C. M. Fan, C. Z. Zhang, A localized space-time method of fundamental solutions for diffusion and convection-diffusion problems, *Adv. Appl. Math. Mech.*, **12** (2020), 940–958.
31. L. Qiu, J. Lin, Q. H. Qin, W. Chen, Localized space-time method of fundamental solutions for three-dimensional transient diffusion problem, *Acta Mech. Sinica-PRC*, **36** (2020), 1051–1057.
32. L. Qiu, F. J. Wang, J. Lin, Q. H. Qin, Q. H. Zhao, A novel combined space-time algorithm for transient heat conduction problems with heat sources in complex geometry, *Comput. Struct.*, **247** (2021), 106495.
33. W. W. Li, Localized method of fundamental solutions for 2D harmonic elastic wave problems, *Appl. Math. Lett.*, **112** (2021), 106759.
34. S. N. Liu, P. W. Li, C. M. Fan, Y. Gu, Localized method of fundamental solutions for two-and three-dimensional transient convection-diffusion-reaction equations, *Eng. Anal. Bound. Elem.*, **124** (2021), 237–244.
35. X. L. Li, S. L. Li, On the augmented moving least squares approximation and the localized method of fundamental solutions for anisotropic heat conduction problems, *Eng. Anal. Bound. Elem.*, **119** (2020), 74–82.
36. W. Z. Qu, C. M. Fan, X. L. Li, Analysis of an augmented moving least squares approximation and the associated localized method of fundamental solutions, *Comput. Math. Appl.*, **80** (2020), 13–30.

37. F. J. Wang, W. Z. Qu, X. L. Li, Augmented moving least squares approximation using fundamental solutions, *Eng. Anal. Bound. Elem.*, **115** (2020), 10–20.
38. X. L. Li, S. L. Li, A linearized element-free Galerkin method for the complex Ginzburg-Landau equation, *Comput. Math. Appl.*, **90** (2021), 135–147.
39. T. Zhang, X. L. Li, Analysis of the element-free Galerkin method with penalty for general second-order elliptic problems, *Appl. Math. Comput.*, **380** (2020), 125306.
40. F. J. Wang, Y. Gu, W. Z. Qu, C. Z. Zhang, Localized boundary knot method and its application to large-scale acoustic problems, *Comput. Methods Appl. Mech. Eng.*, **361** (2020), 112729.
41. F. J. Wang, C. Wang, Z. T. Chen, Local knot method for 2D and 3D convection-diffusion-reaction equations in arbitrary domains, *Appl. Math. Lett.*, **105** (2020), 106308.
42. F. J. Wang, Q. H. Zhao, Z. T. Chen, C. M. Fan, Localized Chebyshev collocation method for solving elliptic partial differential equations in arbitrary 2D domains, *Appl. Math. Comput.*, **397** (2021), 125903.
43. X. X. Yue, F. J. Wang, P. W. Li, C. M. Fan, Local non-singular knot method for large-scale computation of acoustic problems in complicated geometries, *Comput. Math. Appl.*, **84** (2021), 128–143.
44. X. X. Yue, F. J. Wang, C. Z. Zhang, H. X. Zhang, Localized boundary knot method for 3D inhomogeneous acoustic problems with complicated geometry, *Appl. Math. Model.*, **92** (2021), 410–421.
45. P. W. Li, Space-time generalized finite difference nonlinear model for solving unsteady Burgers' equations, *Appl. Math. Lett.*, **114** (2021), 106896.
46. W. Z. Qu, H. He, A spatial-temporal GFDM with an additional condition for transient heat conduction analysis of FGMs, *Appl. Math. Lett.*, **110** (2020), 106579.
47. H. Xia, Y. Gu, Generalized finite difference method for electroelastic analysis of three-dimensional piezoelectric structures, *Appl. Math. Lett.*, **117** (2021), 107084.
48. Z. J. Fu, Z. Y. Xie, S. Y. Ji, C. C. Tsai, A. L. Li, Meshless generalized finite difference method for water wave interactions with multiple-bottom-seated-cylinder-array structures, *Ocean Eng.*, **195** (2020), 106736.
49. T. Belytschko, Y. Krongauz, D. Organ, M. Fleming, P. Krysl, Meshless methods: An overview and recent developments, *Comput. Methods Appl. Mech. Eng.*, **139** (1996), 3–47.

AIMS Press